FAULT LINE DETECTION AND MAPPING FOR EARTHQUAKE USING PHOTOGRAMMETRIC TECHNIQUE WITH GPS/INS EXTERIOR ORIENTATIONS

Kuen-sheng Yeh*[1] and Lien-Huang Chen[2]
[1]Associate Technical Specialist, Aerial Survey Office, Forestry Bureau,
61-3, Chao Chou St., Taipei City 10642, Taiwan; Tel: + 886-2-33432340;
E-mail: d92625003@ntu.edu.tw

[2]Director, Aerial Survey Office, Forestry Bureau
61-3, Chao Chou St., Taipei City 10642, Taiwan; Tel: + 886-2-33437699;
E-mail:clh@mail.afasi.gov.tw

KEY WORDS: Aerial Images, Fault Line Mapping, Aerial Triangulation, Photogrammetry, GPS/INS.

ABSTRACT: A fault line detection method using photogrammetric technique is presented in this paper. The study area includes part of the Chelongpu fault, where drastic displacements were observed during the 1999 Chichi earthquake. Due to lack of GPS/INS data, exterior orientation of earlier aerial images were computed in traditional aerial triangulation procedure to produce the coordinates of feature point set for the study area before the earthquake. Then the coordinates of corresponding point set after earthquake were computed from later aerial images by applying aerial triangulation with GPS/INS data referenced to a fixed GPS base station. By comparing coordinates of the two point sets, the error vectors clearly shows where the fault is. Because points moved along the two sides of the fault with different directions, by densifying and computing the coordinates of common points in the aerial images, the horizontal and vertical displacements can be computed, hence the fault line could be generated more precisely.

1. INTRODUCTION

A fault line can be detected and mapped by geological investigation or by analyzing data such as monitoring station, or point cloud obtained by LiDAR scanner. Geological investigation requires much expenditure of time and effort. LiDAR is a new technique for obtaining large amount of point cloud which contains 3D information that can be used to reconstruct landform digitally. The landform change can be detected by analyzing the point cloud data acquired at different time, and the volumetric change can be estimated (Hsiao, 2006). A disadvantage of LiDAR is that the actual direction and distance of ground movement can not be analyzed because features in point cloud are not easy to identify, nor can the points quality be evaluated. Monitoring a fault by analyzing the data obtained from monitoring station is another alternative to acquire information about direction and distance of land movement, but the quantity and distribution of stations are still insufficient.

To detect a fault line by photogrammetric method is relatively economic since the aerial images were taken annually in Taiwan. Features and objects in aerial images were concrete and can be easily recognized. Furthermore, the ground coordinates of objects in aerial images can be estimated by aerial triangulation. Besides, the digital landform, i.e., the DEMs, can be derived by image auto-matching. In this study, a study area was chosen where the Chi-Chi Earthquake with a magnitude of 7.3 occurred on 21 September 1999, and some obvious surface rupture happened beside the fault line.

Because the origin of map datum moved after the earthquake, the before-and-after datum for aerial triangulation was not the same. The datum for aerial triangulation after earthquake was controlled by some ground control points that were set up after earthquake, but they were far away from the study area. Therefore, Densification were taken and transfer to the aerial images after earthquake as datum.

For additional information of landform change, the DEMs before and after earthquake were generated by image matching and then compared.

2. MATERIALS AND METHOD

2.1 Study Area

The study area has a size of 89.63 Km^2 and is located in the western part of Taiwan between 24° 14′ 51″ N, 24° 20′ 59″ N and 120° 46′ 53″ E, 120° 51′ 34″ E, covering Zhuolan Township and Dongshi District, where the Daan River crosses over. Part of the Chelongpu fault extends from SW to NE (Figure 1).

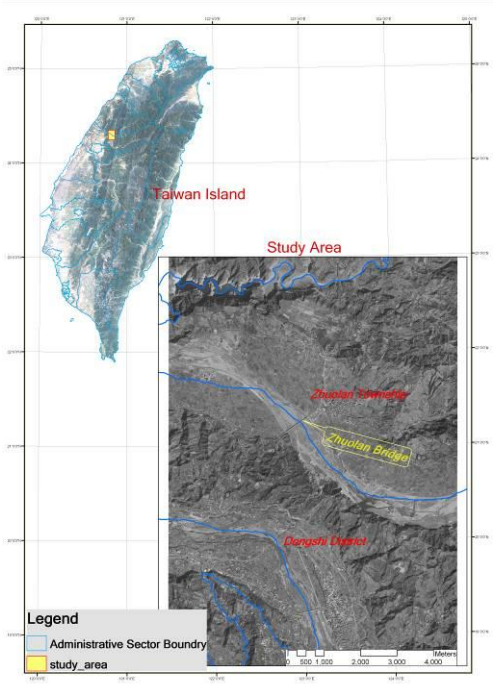

Figure 1 Overview of study area

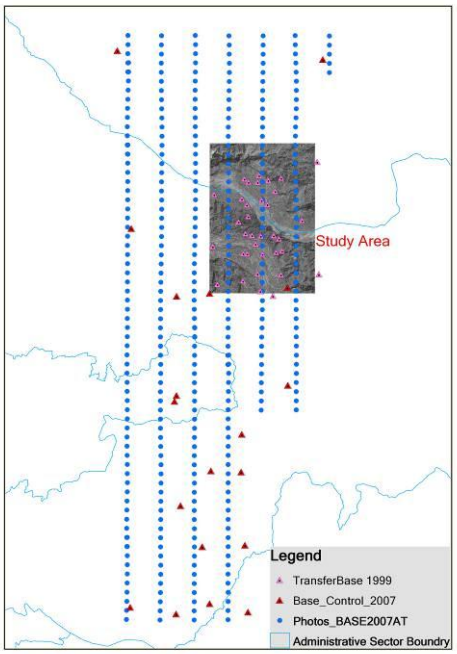

Figure 2 Distribution of aerial images and GCPs for base reference

2.2 Data

Aerial Images And Ground Control Points

Three sets of aerial images were taken and used in this study. The first image set was acquired before the earthquake on 9 April 1998, and the second set was acquired after the earthquake on 18 November 1999. The other set of aerial images was used as base reference which was acquired in 2007, with GPS/INS information recorded at the time of exposure. Distributions of aerial images used and control points are shown in Figure 2, Figure 3, and Figure 4. Source and type of aerial images are shown in Table 1.

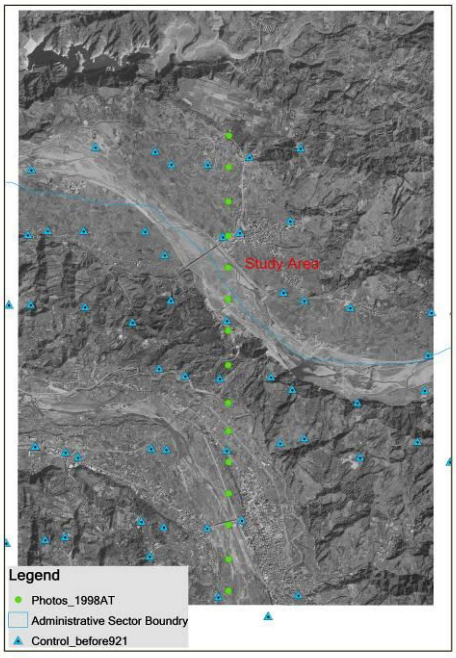

Figure 3 Distribution of aerial images and control points before earthquake

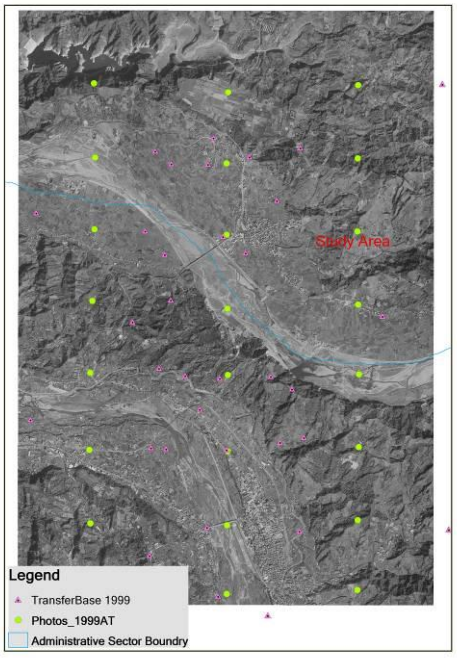

Figure 4 Distribution of aerial images and control points after earthquake

Table 1 Source and type of aerial images

	Aerial Images/Photos Before Earthquake	Aerial Images/Photos After Earthquake	Aerial Images as Base
Camera Type	ZEISS RMKTOP 15	ZEISS RMKTOP 15	Z/I DMC
Image Type	color scanned images	color scanned images	digital sensor images
Focal Length(mm)	152.818	152.818	120
Scan Resolution(um)	14	14	12
Average Flight Height(m)	3500	4000	3300
Date	1998.04.09	1999.11.18	2007.5~2007.11

2.3 Method

Aerial Triangulation

Aerial triangulation is a method used to estimate coordinates of ground objects from aerial images, and it usually combines least square adjustment to optimize the solutions. Recently, a system combining GPS and inertial information has been developed. The GPS offers high absolute accuracy about position and velocity information, and the inertial system offers high accuracy for attitude information. The combined GPS/inertial aerial triangulation is now thought to be the most reliable, flexible and accurate approach (Cramer, 2000). In this study, aerial triangulation with bundle adjustment was applied to obtain coordinates of common objects on aerial images, and to generate more control data if no sufficient ground control exists.

Aerial triangulation for aerial images of 2007 was first conducted with combined GPS/INS information, which can reduce the model deformation when performing aerial triangulation in areas with few ground control points, and help to get reliable estimates of coordinates for objects on images. Objects with estimated coordinates were also treated as control points for aerial images set of 1999 that can offer a relative fixed datum after earthquake because ground control points after earthquake were not enough in the study area.
Datum of aerial images before the earthquake were controlled by aerial triangulation points that were obtained in base map production projects, in which the coordinates of ground control points were measured based on datum before earthquake.

The sigma values for all aerial triangulation projects were limited under 5.0μm.

Displacement of Common Points Before and After Earthquake

Image coordinates of common points before and after earthquake were both recognized and recorded in aerial triangulation project. Aerial triangulations before earthquake and after earthquake were then performed separately using different control point sets. The displacement vectors were than calculated by comparing estimated coordinates of common points before and after the earthquake. It's easy to compare the two coordinates sets by treating the coordinates of objects before earthquake as check points in the after-earthquake aerial triangulation project, and the displacement vectors are shown as error vectors (Figure 5).

In this study, displacements of common points were represented by vectors. The magnitude of horizontal changes was calculated from the Euclidean distance between coordinates before and after earthquake, changes in vertical were represented by height differences. For convenience of plotting and interpreting, the horizontal changes were represented by lengths and directions in horizontal with magnitude multiplied by 40, the vertical changes were represented by circles with radius multiplied by 10. Aerial triangulation can be repeatedly carried out and additional common points were measured if the density of existing common points were not enough to show up the real position of fault line. The final distribution of 236 common points is shown in Figure 6.

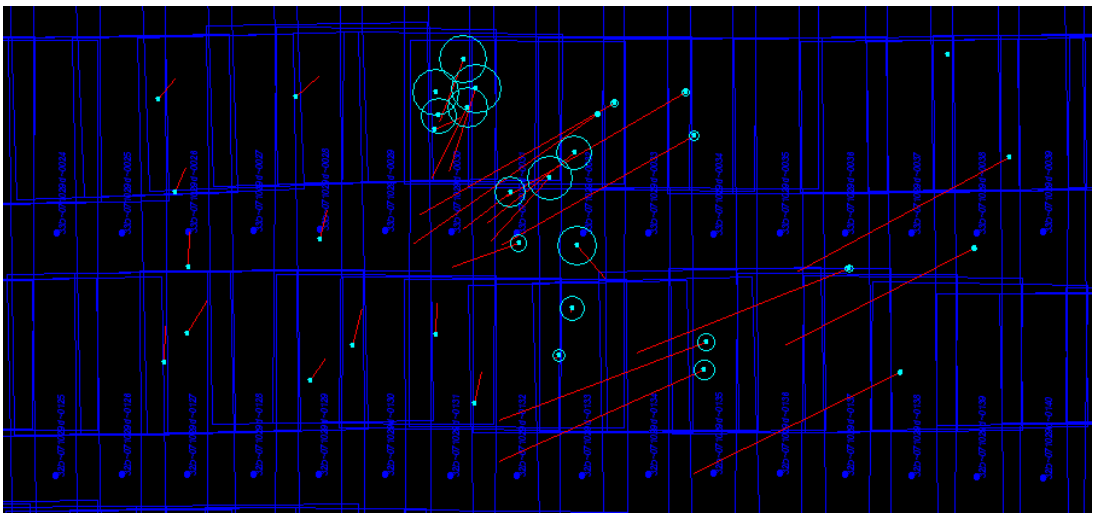

Figure 5 Error vectors in aerial triangulation project

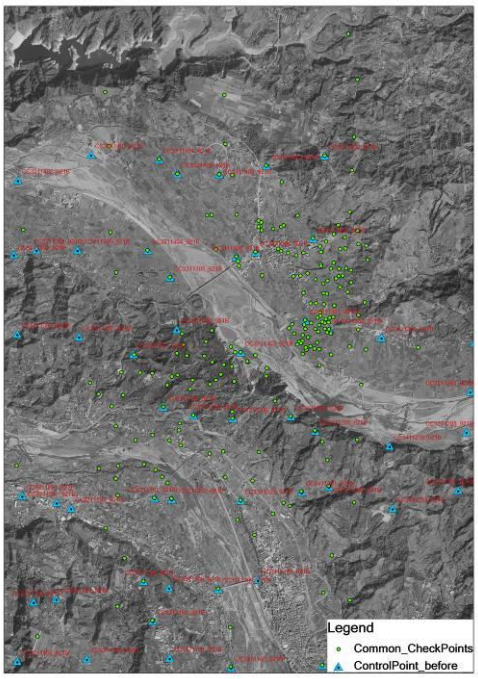

Figure 6 Map of 236 common points

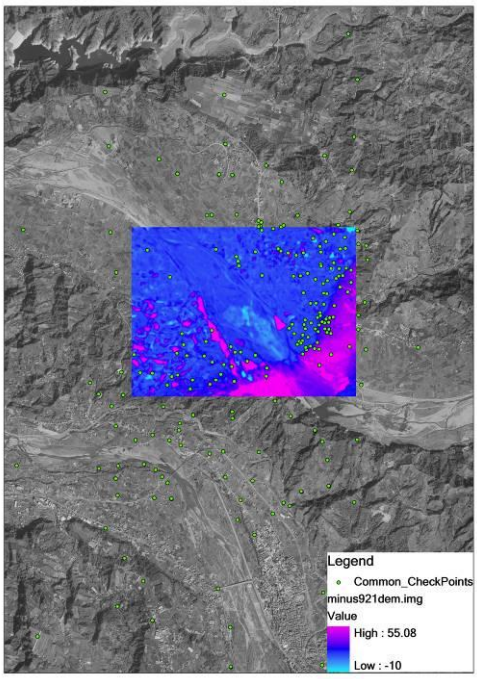

Figure 7 Selected area of change analysis in DEMs

DEMs Before and After Earthquake

The DEMs before and after earthquake near the Zhuolan Bridge were generated by auto-matching, the sampling rate was set to 10m x 10m. All discrete height data were converted to raster format. Finally the change in height of each sample was calculated by subtracting cell value of before-earthquake DEM from after-earthquake DEM. The selected area of change analysis in DEMs is shown in Figure 7.

3. RESULTS

The result of aerial triangulation shows that the accuracy of datum controlled before the earthquake was about 0.24m in horizontal, 0.38m in vertical, with data accuracy of 0.24/0.55 as compared to check points. After the earthquake, the accuracy of datum controlling was about 0.22m in horizontal, 0.86m in vertical, with data accuracy of 0.46m in horizontal, 0.98m in vertical as compared to check points.

The displacement vectors shown in Table 2 are described in component of X, component of Y and component of Z. the given coordinates were the origin of vectors, and the direction and length of vectors in horizontal were calculated from component X and Y.

Table 2 Part of Displacement Vector List

Point_Id	dX	dY	dZ	d(XYZ)	Computed_X	Computed_Y	Computed_Z	Given_X	Given_Y	Given_Z
…	…	…	…	…	…	…	…	…	…	…
…	…	…	…	…	…	…	…	…	…	…
CC023	-3.547	6.217	1.518	7.318	233627.330	2683684.235	376.430	233630.877	2683678.018	374.912
CC024	-2.486	7.634	2.489	8.406	229852.048	2684390.486	387.164	229854.534	2684382.852	384.675
CC027	-3.325	7.827	3.254	9.105	229533.240	2684896.003	324.977	229536.565	2684888.176	321.723
CC028	-3.459	7.642	2.045	8.634	231745.521	2685035.045	315.081	231748.980	2685027.403	313.036
CC029	-4.830	6.865	2.264	8.694	233700.520	2685327.594	440.140	233705.350	2685320.729	437.876
CC030	-2.776	5.552	8.391	10.438	229734.530	2685444.848	324.377	229737.306	2685439.296	315.986
CC031	-3.450	7.584	2.842	8.803	231541.960	2685751.928	340.313	231545.410	2685744.344	337.471
CC034	-2.908	5.042	12.120	13.445	229744.205	2685939.414	304.515	229747.113	2685934.372	292.395
CC035	-3.292	6.626	6.480	9.835	231507.742	2686182.350	335.139	231511.034	2686175.724	328.659
CC036	-4.282	7.422	3.021	9.085	233746.649	2686380.194	479.090	233750.931	2686372.772	476.069
CC038	-1.522	-0.002	10.003	10.118	231656.235	2686841.020	449.784	231657.757	2686841.022	439.781
…	…	…	…	…	…	…	…	…	…	…
…	…	…	…	…	…	…	…	…	…	…

The displacement vectors were then plotted on the map, the result shows that an area around the fault line was easy to be recognized because of the obvious ground displacement. A fault line should go through between displacement vectors with opposite directions. Points with large changes in horizontal were distributed over the south-east of fault line (Figure 8), and points with large changes in vertical were distributed in a zone beside the fault line (Figure 9).

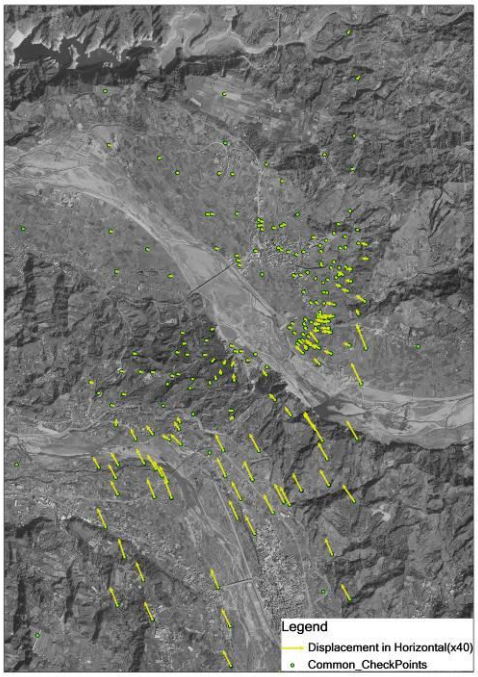

Figure 8 Displacement vectors in horizontal

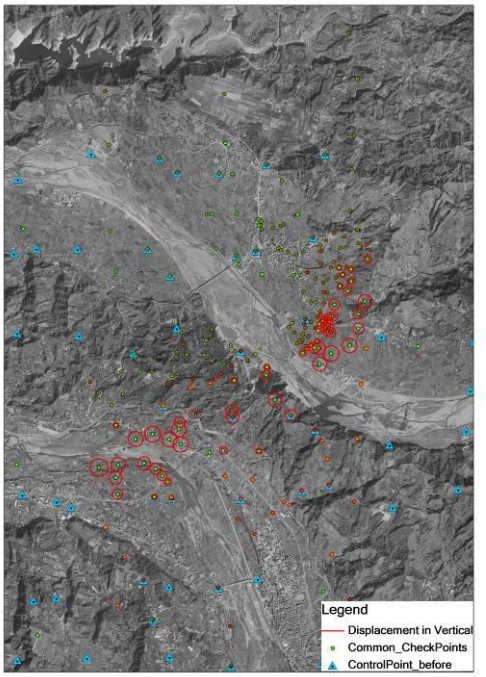

Figure 9 Displacement vectors in vertical

By comparing the 10m x 10m DEMs before and after the earthquake, a erupted zone was recognized easily by symbolizing the height differences with shaded colors. The erupted zone was moved upward with a maximum of 14 meters displacement after the earthquake, the south side of the erupted zone in the study area was moved greatly in north-west direction, whereas the north side was moved slightly in south-east direction (Figure 10).

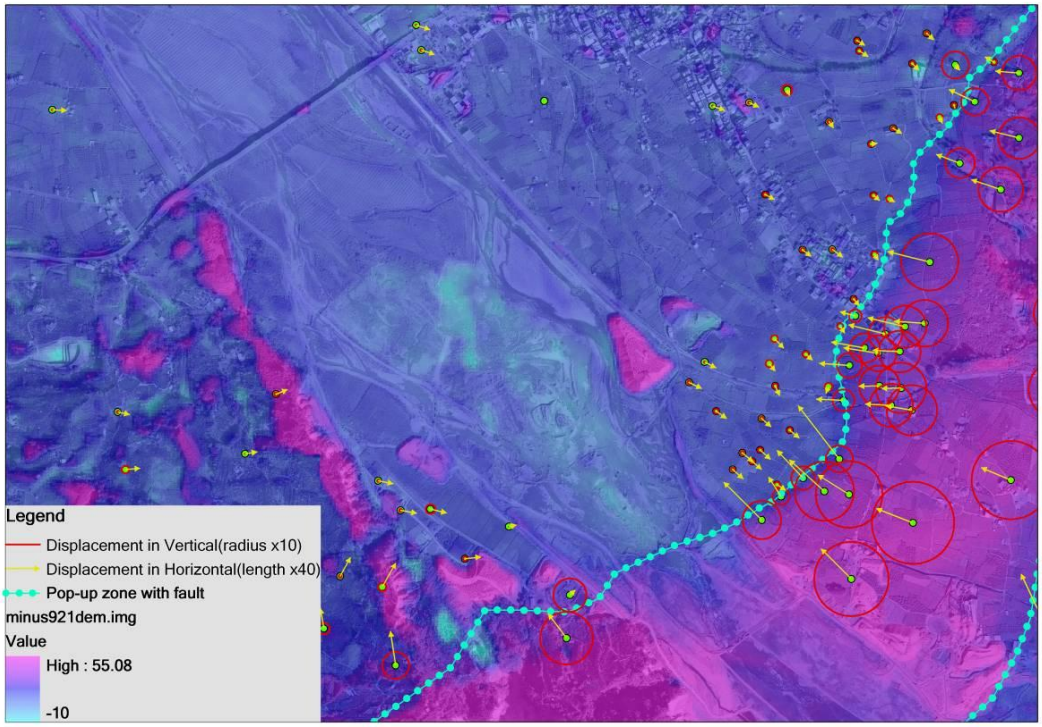

Figure 10 Vertical differences in DEMs represented with shaded map which shows the erupted area and a fault line

4. CONCLUSION

To compare spatial data derived from aerial images acquired in different time periods, it's important to decide a relative fixed base datum. Photogrammetric method with GPS/INS information can be used to estimate the coordinates of objects on images with fewer ground control points that are identical in datum.

This study offers an effective method to detect the fault line more precisely, and with more displacement details near the fault line. The study also shows that the active fault line could be roughly detected during the aerial triangulation procedure. Moreover, the more common tie points or pass points before and after earthquake were measured, the better accuracy of the fault line and ground movement in earthquake can be detected.

The DEMs before and after earthquake can also be generated by image matching. It also offers a way to detect the fault line morphologically and efficiently, which can generate a more smoothly fault line or fault zone.

Another advantage of applying photogrammetry in fault line detection is that corresponding orthoimages could be produced if necessary before the further investigations.

5. References

Cramer M., 2001. On the use of direct georeferencing in airborne photogrammetry. Proceedings 3rd. International Symposium on Mobile Mapping Technology, Cairo, Egypt.

Cramer M., Dirk S., Norber H., 2000. Direct georeferencing using GPS/Inertial exterior orientations for photogrammetric applications, International Archives of Photogrammetry and Remote Sensing, v. 33, part B3, pp. 198-205

Hsiao K. H., J. K. Liu, D. K. Cheng, M. F. Yu, W. C. Hsu, C. L. Wang, 2006. Terrain change detection combined photogrammetric DEM and airborne LIDAR data, Journal of Photogrammetry and Remote Sensing, Vol. XI, No.3, pp.283-295.